

Unraveling Urban NO_x Emission Sources in Polluted Arctic Wintertime Using NO₂ Nitrogen Isotopes

Key Points:

- A temporal variability in NO₂ nitrogen isotopes is measured during winter in downtown Fairbanks, Alaska
- Isotope exchange fractionation drives NO₂ nitrogen isotope distribution, at a rate in excellent agreement with theoretical predictions
- A¹⁵N-based source apportionment indicates vehicle and oil space heating emissions are the main sources of NO_x in downtown Fairbanks

Supporting Information:

Supporting Information may be found in the online version of this article.

Correspondence to:

S. Albertin,
sarah.albertin@noaa.gov

Citation:

Albertin, S., Bekki, S., Savarino, J., Brett, N., Law, K. S., Cesler-Maloney, M., et al. (2024). Unraveling urban NO_x emission sources in polluted Arctic wintertime using NO₂ nitrogen isotopes. *Journal of Geophysical Research: Atmospheres*, 129, e2024JD041842. <https://doi.org/10.1029/2024JD041842>

Received 24 JUN 2024

Accepted 21 SEP 2024

Corrected 16 NOV 2024

This article was corrected on 16 NOV 2024. See the end of the full text for details.

Author Contributions:

Conceptualization: Sarah Albertin, Slimane Bekki, Joël Savarino





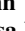


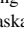




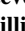

Data curation: Natalie Brett, Meeta Cesler-Maloney, James H. Flynn, Fangzhou Guo

Formal analysis: Sarah Albertin, Natalie Brett, Soline Richard

Funding acquisition: Joël Savarino, Kathy S. Law, Nicolas Caillon, Becky Alexander, Steve R. Arnold, Stefano Decesari, Gilberto J. Fochesatto, Jingqiu Mao, William Simpson

© 2024 The Author(s).

This is an open access article under the terms of the [Creative Commons Attribution-NonCommercial License](#), which permits use, distribution and reproduction in any medium, provided the original work is properly cited and is not used for commercial purposes.

Sarah Albertin^{1,2,3} , Slimane Bekki², Joël Savarino¹ , Natalie Brett^{2,4} , Kathy S. Law² , Meeta Cesler-Maloney⁵ , James H. Flynn⁶ , Fangzhou Guo^{6,7} , Brice Barret⁸, Nicolas Caillon¹ , Barbara D'Anna⁹, Elsa Dieudonné¹⁰, Alexis Lamothe¹ , Soline Richard¹, Brice Temime-Roussel⁹, Becky Alexander¹¹ , Steve R. Arnold⁴ , Stefano Decesari¹² , Gilberto J. Fochesatto¹³, Jingqiu Mao⁵ , and William Simpson⁵ 

¹University Grenoble Alpes, CNRS, IRD, INRAE, Grenoble INP, IGE, Grenoble, France, ²Sorbonne Université, UVSQ, CNRS, LATMOS/IPSL, Paris, France, ³Now at Cooperative Institute for Research in Environmental Sciences, University of Colorado / Chemical Sciences Laboratory, National Oceanic and Atmospheric Administration, Boulder, CO, USA,

⁴School of Earth and Environment, University of Leeds, Leeds, UK, ⁵Geophysical Institute and Department of Chemistry and Biochemistry, University of Alaska Fairbanks, Fairbanks, AK, USA, ⁶Earth & Atmospheric Sciences, University of Houston, Houston, TX, USA, ⁷Now at Aerodyne Research Inc, Billerica, MA, USA, ⁸Université Toulouse III – Paul Sabatier, CNRS, LAERO, Toulouse, France, ⁹Aix Marseille University, CNRS, LCE, Marseille, France, ¹⁰Laboratoire de Physico-Chimie de l'Atmosphère, Université du Littoral Côte d'Opale, Dunkerque, France, ¹¹Department of Atmospheric Sciences, University of Washington, Seattle, WA, USA, ¹²CNR-ISAC, National Research Council of Italy, Institute of Atmospheric Sciences and Climate, Bologna, Italy, ¹³Department of Atmospheric Sciences, College of Natural Science and Mathematics, University of Alaska, Fairbanks, AK, USA

Abstract Nitrogen (N) isotopic fractionation during nitrogen oxides (NO_x) cycling and conversion into atmospheric nitrate alters the original N isotopic composition ($\delta^{15}\text{N}$) of NO_x emissions. Limited quantification of these isotopic effects in urban settings hampers the $\delta^{15}\text{N}$ -based identification and apportionment of NO_x sources. $\delta^{15}\text{N}$ of nitrogen dioxide (NO₂) measured during winter in downtown Fairbanks, Alaska, displayed a large temporal variability, from -10.2 to 24.1‰ . $\delta^{15}\text{N}(\text{NO}_2)$ records are found to be driven by equilibrium isotopic fractionation, at a rate in very close agreement with theoretical predictions. This result confirms that N isotopic partitioning between NO and NO₂ can be accurately predicted over a wide range of conditions. This represents an important step for inferring NO_x emission sources from isotopic composition measurement of reactive nitrogen species. After correcting our $\delta^{15}\text{N}(\text{NO}_2)$ measurements for N fractionation effects, a $\delta^{15}\text{N}$ -based source apportionment analysis identifies vehicle and space heating oil emissions as the dominant sources of breathing-level NO_x at this urban site. Despite their large NO_x emissions, coal-fired power plants with elevated chimney stacks (>26 m) appear to make a small contribution to surface NO_x levels in downtown Fairbanks (likely less than 18% on average). The combined uncertainties of the $\delta^{15}\text{N}$ of NO_x from heating oil combustion and of the influence of low temperatures on the $\delta^{15}\text{N}$ of NO_x emitted by vehicle exhaust prevent a more detailed partitioning of surface NO_x sources in Fairbanks.

Plain Language Summary Nitrogen (N) stable isotopes measured in atmospheric reactive N (N_r) species can help trace emission sources of nitrogen oxides (NO_x). However, large uncertainties subsist regarding the factors controlling the variability of N isotopes in N_r species, preventing a precise isotope-based emission source apportionment. This study presents a comprehensive analysis of the enrichment of ¹⁵N–¹⁴N ($\delta^{15}\text{N}$) in atmospheric nitrogen dioxide (NO₂) collected during the Alaskan Layered Pollution And Chemical Analysis (ALPACA) 2022 international winter campaign in Fairbanks, Alaska. Building on in situ meteorological and trace gas, the isotopic fractionation effect driving the significant $\delta^{15}\text{N}$ variability of NO₂ observed in downtown Fairbanks is quantified with great precision. The $\delta^{15}\text{N}$ records corrected for equilibrium fractionation effects are discussed in light of a local NO_x emission inventory. In particular, the influence of emissions from coal-fired power plants with high stack heights on surface air pollution is addressed.

1. Introduction

Once emitted into the atmosphere, nitrogen oxides (NO_x \equiv nitrogen monoxide (NO) + nitrogen dioxide (NO₂)) rapidly enter an interconversion photochemical cycle (R1–R4). Briefly, NO is oxidized by ozone (O₃; R1) and

Investigation: Sarah Albertin, Alexis Lamothe
Methodology: Sarah Albertin, Slimane Bekki, Joël Savarino
Project administration: Kathy S. Law, Nicolas Caillon, Becky Alexander, Steve R. Arnold, Stefano Decesari, Gilberto J. Fochesatto, Jingqiu Mao, William Simpson
Resources: Meeta Cesler-Maloney, James H. Flynn, Fangzhou Guo
Supervision: Slimane Bekki, Joël Savarino
Validation: Nicolas Caillon
Writing – original draft: Sarah Albertin
Writing – review & editing: Slimane Bekki, Joël Savarino, Natalie Brett, Kathy S. Law, Brice Barret, Barbara D'Anna, Elsa Dieudonné, Alexis Lamothe, Brice Temime-Roussel, Becky Alexander, Steve R. Arnold, Stefano Decesari

peroxy radicals ($\text{RO}_2 \equiv$ hydroperoxyl radical (HO_2) + methyl peroxy radical (CH_3O_2); **R2**), followed by the photolysis of NO_2 (**R3**), leading back to the production of NO and O_3 (**R4**) (Crutzen, 1970):



During the day, at mid-latitudes, NO and NO_2 interconvert so rapidly that a photostationary steady state is usually established within a few minutes (Leighton, 1961). This NO_x cycling plays an important role in the tropospheric oxidation capacity through direct and indirect regulation of key atmospheric trace gases such as O_3 and the hydroxyl radical (OH). A large share of NO_x is ultimately converted into atmospheric nitrate ($\text{NO}_3^- \equiv$ nitric acid + particulate nitrate), with cascade effects on biodiversity, water quality, human health, and the climate (Galloway et al., 2008; Sutton et al., 2011; Szopa et al., 2021; Vitousek et al., 1997; WHO, 2021).

Identifying the origins of NO_3^- gaseous precursors is central to developing effective environmental mitigation policies, particularly in urban settings where NO_3^- is a major component of fine particulate matter ($\text{PM}_{2.5}$) (R. Zhang et al., 2015). For this purpose, the use of nitrogen (N) stable isotopic enrichments in NO_3^- , noted $\delta^{15}\text{N}$ (NO_3^-) ($\delta^{15}\text{N} = (^{15}\text{N}/^{14}\text{N})_{\text{sample}} / (^{15}\text{N}/^{14}\text{N})_{\text{N}_2\text{-air}} - 1$) and expressed in per mill (‰), has attracted growing interest in recent years (e.g., Altieri et al., 2022; Lim et al., 2022; Song, Liu, Hu, et al., 2021; Song, Liu, & Liu, 2021; Xiao et al., 2023; W. Zhang et al., 2022). This approach relies on the distinctive $\delta^{15}\text{N}$ value of the NO_x emitted, arising from the different N isotopic fractionations that occur during the NO_x emission processes (Felix et al., 2012; D. J. Miller et al., 2017, 2018; Walters, Tharp, et al., 2015; Walters, Goodwin, & Michalski, 2015). However, further ^{15}N partitionings occur during the conversion of NO_x to NO_3^- , notably during the NO_x cycle (**R1–R4**) (Li et al., 2020). These isotopic effects fall into three categories: (a) The equilibrium isotope effect (EIE), (b) the kinetic isotope effect (KIE), and (c) the photochemical isotope fractionation effect (PHIFE) (C. E. Miller & Yung, 2000; Young et al., 2002). Based on the isotopic mass balance equation, the resulting $\delta^{15}\text{N}$ of NO_2 ($\delta^{15}\text{N}(\text{NO}_2)$) can be expressed as a function of a factor F_N , expressed in ‰, representing the overall N isotopic fractionation effect between NO_x emissions and NO_2 , the fraction of NO_x in the form of NO_2 ($f_{\text{NO}_2} = \frac{\text{NO}_2}{\text{NO} + \text{NO}_2}$), and the $\delta^{15}\text{N}$ value of ambient NO_x ($\delta^{15}\text{N}(\text{NO}_x)$) (Albertin et al., 2021; Freyer et al., 1993; Li et al., 2020; Walters et al., 2018):

$$\delta^{15}\text{N}(\text{NO}_2) = F_N \times (1 - f_{\text{NO}_2}) + \delta^{15}\text{N}(\text{NO}_x) \quad (1)$$

$\delta^{15}\text{N}(\text{NO}_x)$ can be approximated by a linear combination of the individual source $\delta^{15}\text{N}$ values weighted by the relative contributions of individual sources to the total NO_x as

$$\delta^{15}\text{N}(\text{NO}_x) \approx \sum_i (f_i \times \delta^{15}\text{N}(\text{NO}_{x,i})) \quad (2)$$

with f_i the relative contribution of the NO_x emission source i ($f_i = \frac{E_i}{E_{\text{TOT}}}$ with E_i the NO_x from the source i and E_{TOT} the total NO_x , with $\sum_i f_i = 1$) and $\delta^{15}\text{N}(\text{NO}_{x,i})$ their associated mean isotopic signature. F_N is intricately governed by EIE, KIE, and PHIFE, with the importance of each effect determined by local conditions such as temperature, NO_x – O_3 regime, and solar radiation (Albertin et al., 2021; Freyer et al., 1993; Li et al., 2020; Walters et al., 2016). Therefore, using the $\delta^{15}\text{N}$ content of NO_3^- for the direct identification of the nature of gaseous precursors after emission requires a clear understanding and quantification of these fractionation effects which remain poorly determined. A large part of this knowledge gap stems from the lack of quantification in the N fractionation by NO_x cycling, with very few comparisons between laboratory-derived and theoretical N fractionation factors and ambient isotopic observations (Albertin et al., 2021, 2024; Freyer et al., 1993; Li et al., 2020; Walters et al., 2018).

In their pioneering work, Freyer et al. (1993) first identified a N isotope exchange equilibrium between NO and NO₂ under polluted conditions in Germany. They demonstrated that EIE predominantly influenced the atmospheric $\delta^{15}\text{N}$ record of NO_x (varying from ca. −6 to 6‰ over 1 year). The EIE isotope fractionation factor between NO and NO₂ ($\alpha_{\text{EIE}(\text{NO}_2/\text{NO})}$) is strongly temperature-dependent and can be theoretically derived using harmonic oscillator frequencies (Begun & Fletcher, 1960; Monse et al., 1969; Walters & Michalski, 2015). Chamber experiments also allow for the determination of $\alpha_{\text{EIE}(\text{NO}_2/\text{NO})}$ in controlled conditions (Begun & Melton, 1956; Li et al., 2020; Walters et al., 2016). Only three recent studies have addressed the issue of isotopic exchanges between NO and NO₂ in atmospheric conditions (Albertin et al., 2021, 2024; Walters et al., 2018). Notably, as in Freyer et al. (1993), Albertin et al. (2024) found significant EIE between emitted NO_x and NO₂ in an Alpine urban atmosphere. The authors observed an isotopic exchange of $(43.6 \pm 3.3)\%$ in good agreement with that derived from the Walters and Michalski (2015) theoretical approach at $(42.3 \pm 1.3)\%$. If the uncertainties associated with the use of $\delta^{15}\text{N}$ measured in NO₃[−] for source apportionment are to be reduced, more quantitative studies are required on the N fractionation effects in reactive nitrogen species. Meanwhile, the applicability of quantifying N isotopic fractionation using theoretical calculations needs to be tested over a wide range of temperatures and pollution conditions.

Expanding on Albertin et al. (2024), NO₂ was sampled in an urban Arctic environment in winter 2022 in Fairbanks, Alaska to measure its N isotopic composition. Fairbanks winter conditions (i.e., low temperatures, weak insolation, and high NO_x) provide an ideal extreme setting to test our understanding of N exchanges in the NO_x cycle and evaluate theoretical approaches. This study was conducted as part of the joint ALPACA (Alaskan Layered Pollution and Chemical Analysis) and CASPA (Climate-relevant Aerosol Sources and Processes in the Arctic) projects focusing on emission source identification and physicochemical processes leading to severe pollution events during the winter in Fairbanks, as well as their links to boundary layer dynamics (Simpson et al., 2024). Building on meteorological and trace gas observations, this study identifies factors influencing $\delta^{15}\text{N}$ measured in NO₂. For the first time, N isotopic fractionations observed during NO_x cycling in an urban and polar environment are confronted with theoretical estimates. After correction for equilibrium isotope exchange, the dominant NO_x emission sources influencing the sampling site are examined using isotopic records and a local emission inventory.

2. Materials and Methods

2.1. Sampling and Isotopic Analysis

Ambient NO₂ was sampled periodically over January–February 2022 in downtown Fairbanks, Alaska near the University of Alaska Fairbanks (UAF) Community and Technical College (CTC) building (64°50′27″N 147°43′34″W, 135 m above sea level). The CTC site is surrounded by roads, a residential area, the business district, and several power plants providing energy (Figure S1 in Supporting Information S1).

Thirty three samples were collected over 6 distinct sampling periods at ground level on denuder tubes inserted in series within a speciation cartridge (ChemComb® 3500, Thermo Scientific®, USA) connected to an off-line gas sampler ($\approx 10 \text{ L min}^{-1}$ at standard temperature and pressure conditions). Coated with an alkaline guaiacol mixture, denuders allow for quantitative collection of NO₂ (Nash, 1970) under varying temperature and relative humidity conditions while preserving the integrity of NO₂ isotopes (Albertin et al., 2021; Blum et al., 2023; Walters et al., 2018; Zhou et al., 2022). Over six distinctive sampling periods, 33 denuder sets were performed, with collection times ranging from 3 to 9 hr (procedure strictly identical to that detailed in Albertin et al., 2024). Nitrite (NO₂[−]) formed from the reaction of NO₂ with the guaiacol coating was extracted in 10 mL of ultrapure water ($18.2 \text{ M}\Omega \text{ cm}^{-1}$) under ultraclean conditions at the UAF laboratory. Sample extractions were stored frozen and shipped to the Institut des Géosciences de l'Environnement (Grenoble, France) isotopic laboratory for subsequent analysis. Trace gases (NO, NO₂ and O₃) and meteorological parameters (ambient temperature at 3 and 11 m) were measured continuously at CTC throughout the field ALPACA-2022 campaign from 17 January to 25 February (see description in Simpson et al. (2024)).

NO₂[−] concentration in denuder extractions was estimated using UV-Vis spectrometry at 544 nm (Griess-Saltzman reaction). The contribution of NO₂[−] from blank denuders was almost always found to be negligible ((mean ± 1 standard deviation) = $(0.9 \pm 1.4)\%$). NO₂[−] from the denuders in second position represented on average $(1.8 \pm 1.4)\%$ of the total NO₂[−] measured on the first denuders. N isotope ratios ($^{15}\text{N}/^{14}\text{N}$) of NO₂[−] were

measured using the azide method (McIlvin & Altabet, 2005). NO_2^- was converted into nitrous oxide (N_2O) using a sodium azide/acetic acid buffer solution. N_2O was then thermally decomposed into N_2 and O_2 in a gold tube (Kaiser et al., 2007) and analyzed for isotopic composition on a Thermo Finnigan MAT253 Isotope Ratio Mass Spectrometer (continuous flow mode) equipped with gas chromatography (GasBench IITM) (Morin et al., 2009). When possible, NO_2^- analytes were analyzed several times (Table S1 in Supporting Information S1). International standard salts used to calibrate $\delta^{15}\text{N}$ isotopic ratios (Table S2 in Supporting Information S1) had an average standard deviation of $\pm 0.2\text{‰}$. The analytical procedure used for this study is strictly identical to the description given in Albertin et al. (2021).

2.2. ADEC/EPA NO_x Emission Inventory

The Alaska Department of Conservation (ADEC)/Environmental Protection Agency (EPA) reproduced an updated emission inventory for the duration of the ALPACA-2022 campaign, including NO_x emissions at the surface within the Fairbanks nonattainment area at hourly time resolution and emissions from power plants located in the Fairbanks area (Figure S1 in Supporting Information S1). The contribution from power plant emissions to surface pollution is a key issue in Fairbanks during winter, as the exhaust chimneys are often above the surface inversion layer (Simpson et al., 2024). We distinguish here between emissions from diesel and coal-fired power plants, which are referred to as diesel-PP and coal-PP. For our study, surface NO_x emissions are grouped by sectors for: space heating (residential and commercial) and fuel type combustion: oil, wood, and fossil gas (negligible emissions from coal combustion for space heating are excluded). Vehicle exhaust combines on-road and non-road emissions. Surface emissions from industrial waste oils, airport activities, and minor point sources resulting from a combination of oil and gas combustion grouped under the term “other sources”. See ADEC (2019a) and Brett et al. (2024) for details about the emission inventory.

3. Results and Discussion

3.1. Atmospheric Observations

Classified as a serious $\text{PM}_{2.5}$ nonattainment area in 2017 (ADEC, 2019b), Fairbanks-North Star Borough experiences severe winter air pollution (Cesler-Maloney et al., 2022; Fochesatto et al., 2015; Mayfield & Fochesatto, 2013; Robinson et al., 2023; Tran & Mölders, 2011). High winter pollution is linked to weak vertical mixing, especially during surface-based temperature inversions (SBIs) events, when pollutant emissions can accumulate for hours to days near the surface. Strong SBIs have been defined by temperature differences between 3 and 11 m ($dT_{11\text{m}-3\text{m}}$) greater than 0.5°C (Cesler-Maloney et al., 2022). In such conditions, surface O_3 is generally fully titrated by NO (R1). In weakly stable conditions, SBIs collapse (i.e., $dT_{11\text{m}-3\text{m}} < 0.5^\circ\text{C}$) and O_3 increases due to transport from aloft and NO_x dilution. During the ALPACA-2022 field study, two extreme pollution episodes were observed, from January 29 to February 3, and from February 23 to February 25 (Simpson et al., 2024).

The NO_2 sampling strategy aimed to cover distinct pollution conditions during the campaign. Four NO_2 sampling periods correspond to moderately polluted (MP) periods (from January 25 to 26 = MP#1, from February 8 to 9 = MP#2, from February 11 to 12 = MP#3, and from February 16 to 17 = MP#4; Figure 1). During these MP periods, NO_2 , NO , and O_3 mixing ratios fluctuate, with no clear diurnal patterns but in a correlated way. In short, when NO and NO_2 increase, O_3 decreases substantially, and vice versa (Figure 1). NO_2 mixing ratios range from ca. 1 to 49 nmol mol^{-1} during the MP periods with a mean ± 1 standard deviation of $(22.5 \pm 15.2) \text{ nmol mol}^{-1}$. O_3 mixing ratios reach a maximum of $35.2 \text{ nmol mol}^{-1}$ in the early morning during MP#1, typical of wintertime background air at high latitudes (Whaley et al., 2023). NO_2 sampling was also carried out during the two extremely polluted (EP) periods (from January 29 to February 2 = EP#1, and from February 24 to 25 = EP#2). EP#1 is considered the “cold pollution event” of the field campaign (Simpson et al., 2024). The temperature drops to -35°C and $\text{PM}_{2.5}$ levels reach their maximum (Figure S2 in Supporting Information S1). In contrast, although still highly polluted, EP#2 is much warmer, with temperatures above freezing. NO_x mixing ratios are elevated during both periods (mean of $(130.9 \pm 38.1) \text{ nmol mol}^{-1}$) with NO being the dominant NO_x component (i.e., low f_{NO_2}), and O_3 being almost or fully titrated (Figure 1). Covering different temperature and pollution conditions, the six NO_2 sampling periods can be considered representative of the diverse conditions encountered throughout the ALPACA-2022 campaign (Figure S2 in Supporting Information S1).

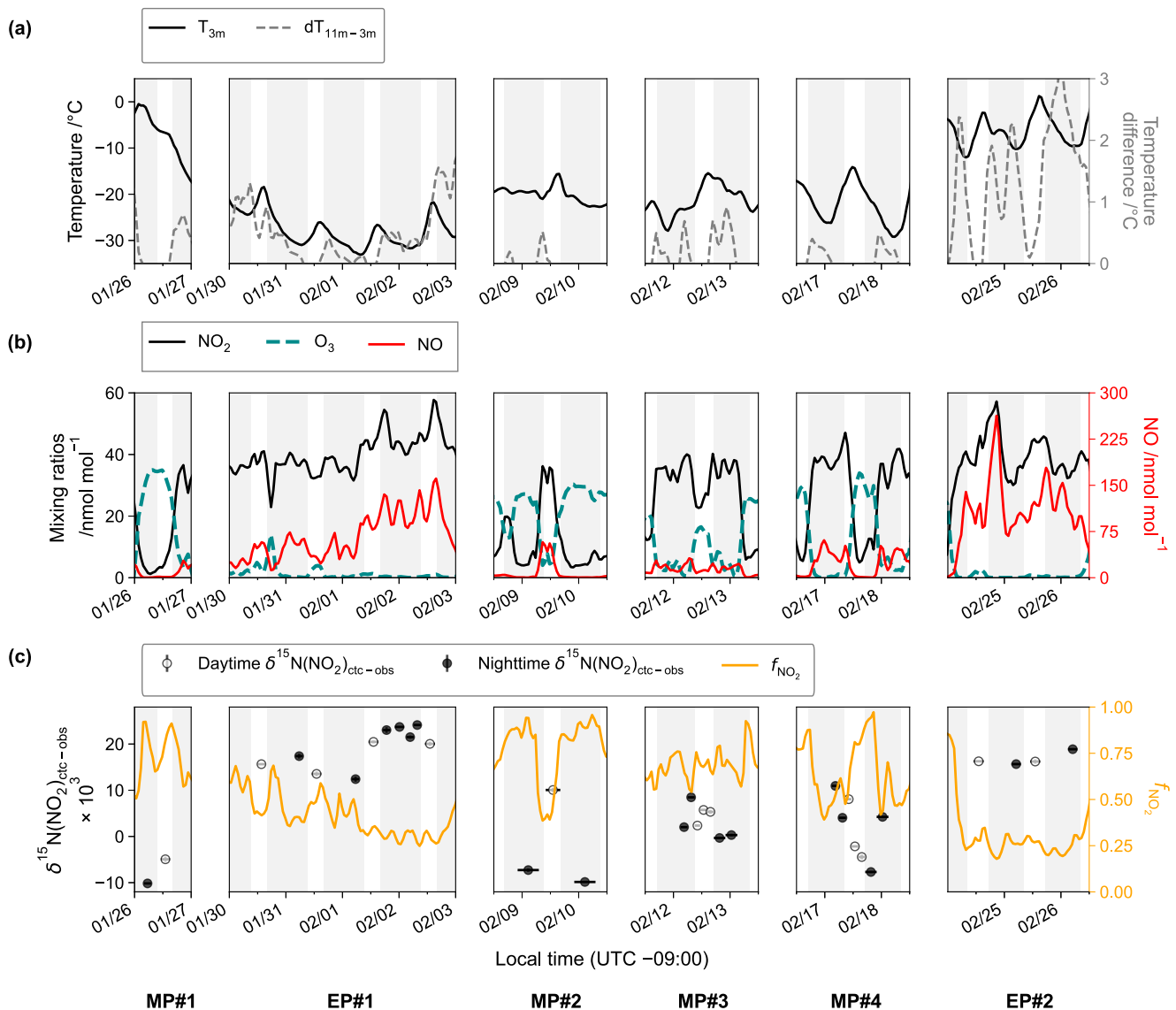


Figure 1. Panel (a) displays temperature at 3 m (black line) and the temperature difference between 11 and 3 m (gray dashed line) at CTC. Panel (b) displays the 2-hr rolling mean of NO_2 (black line), O_3 (cyan dashed line), and NO (red line) mixing ratios measured at CTC during 6 non continuous periods (MP = moderately polluted and EP = extremely polluted). Panel (c) displays $\delta^{15}\text{N}$ of atmospheric NO_2 (white and black dots for daytime and nighttime values, respectively) measured at CTC and the ratio f_{NO_2} (orange line). The horizontal bars of the isotopic data cover the NO_2 collection time and the dots represent the middle of the sampling period. Gray backdrop shaded areas represent the night duration. $\delta^{15}\text{N}(\text{NO}_2)_{\text{ctc-obs}}$ values and atmospheric observations averaged over each denuder collection interval are reported in Table S1 and S3 in Supporting Information S1, respectively.

3.2. N Fractionation Effects

$\delta^{15}\text{N}$ of atmospheric NO_2 at CTC ($\delta^{15}\text{N}(\text{NO}_2)_{\text{ctc-obs}}$) fluctuates markedly over the six sampling periods (Figure 1b), ranging from -10.2 to 24.1‰ (weighted average of $12.3 \pm 11.1\text{‰}$). Day (09:00–17:20 local time) and night (17:20–09:00 local time) $\delta^{15}\text{N}$ values do not differ very significantly (independent samples t -test p -value of 0.8). $\delta^{15}\text{N}(\text{NO}_2)_{\text{ctc-obs}}$ values mainly fall within the range of previous measurements in suburban/urban environments, ranging from -31 to 20‰ (Albertin et al., 2021, 2024; Freyer et al., 1993; Walters et al., 2018).

It is now well established that the variability in $\delta^{15}\text{N}(\text{NO}_2)$ can be attributed to two different causes: (a) Changes in the nature and relative contribution of NO_x emission sources and (b) partitioning of ^{15}N between NO and NO_2 due to fractionation effects. As expected from Equation 1, $\delta^{15}\text{N}(\text{NO}_2)_{\text{ctc-obs}}$ correlates well with $(1 - f_{\text{NO}_2})$, the fraction of NO_x under the form of NO ($R^2 = 0.9$, $p < 0.05$, $n = 33$; Figure 2a). This linear relationship indicates that the variability of $\delta^{15}\text{N}(\text{NO}_2)$ at CTC is primarily driven by isotopic fractionation effects. Additionally, the

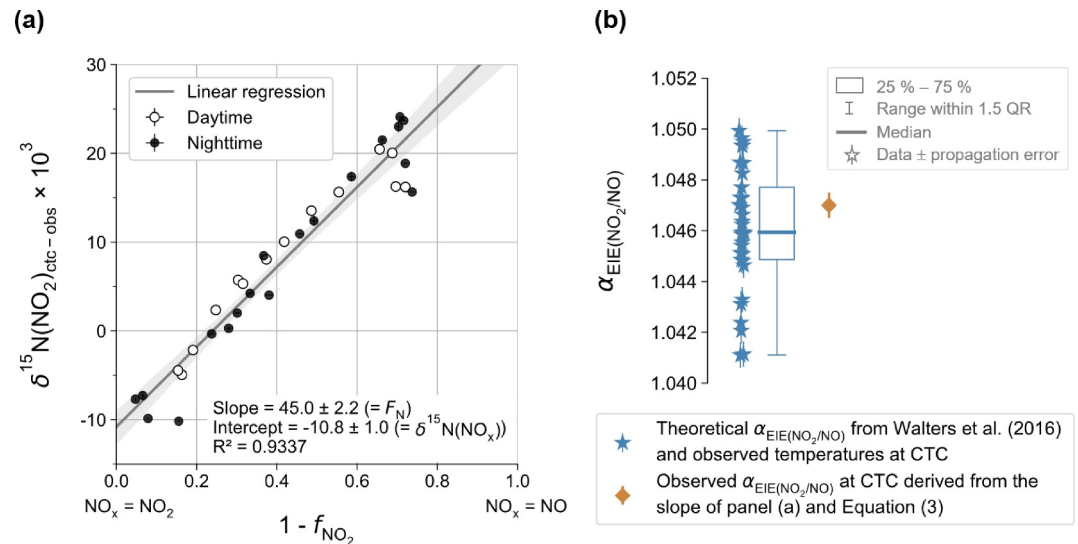


Figure 2. (a) $\delta^{15}\text{N}$ of atmospheric NO_2 (vertical axis, in ‰) as a function of $(1 - f_{\text{NO}_2})$ (horizontal axis) from observations at the CTC site, Fairbanks, Alaska, in January–February 2022. f_{NO_2} is averaged over the collection period of each NO_2 sample. White and black dots represent daytime and nighttime data, respectively. The gray shading is the 95% confidence interval. Panel (b) shows theoretical $\alpha_{\text{EIE}(\text{NO}_2/\text{NO})}$ during individual NO_2 collection periods, derived from Walters et al. (2016) approach (Equation 4) and observed temperatures in Fairbanks (blue stars). The spread of the theoretical $\alpha_{\text{EIE}(\text{NO}_2/\text{NO})}$ values results from the temperature variability during NO_2 sampling periods (from -32.5°C to -1.6°C). The brown diamond represents the mean observed $\alpha_{\text{EIE}(\text{NO}_2/\text{NO})}$ during the NO_2 sampling periods, derived from the slope of panel (a) and Equation 3.

$\delta^{15}\text{N}$ value of NO_x emissions, represented by the intercept of the fit ($\delta^{15}\text{N}(\text{NO}_x)_{\text{ctc-obs}} = (-10.8 \pm 1.0)\text{‰}$), remains constant throughout the campaign. As this linear dependency between $\delta^{15}\text{N}(\text{NO}_2)_{\text{ctc-obs}}$ and $(1 - f_{\text{NO}_2})$ applies to both day and night samples, similar isotopic processes governing the $\delta^{15}\text{N}(\text{NO}_2)_{\text{ctc-obs}}$ variability are expected over the diurnal cycle.

As mentioned above, N fractionation effects, grouped under the term F_N and represented here by the linear regression slope in Figure 2a, encompass the different natures of isotopic partitioning in the NO_x cycle, that is, PHIFE, KIE and EIE. As detailed in Li et al. (2020), the relative contribution of each isotopic fractionation effect is expected to differ between a remote and a heavily polluted atmosphere. On the one hand, in clean environments, NO_x is mainly in the form of NO_2 due to efficient oxidation, notably by O_3 . Hence, the NO_2 chemical lifetime (where $\tau_{\text{chem-NO}_2} = \frac{1}{J_{\text{NO}_2}}$, with J_{NO_2} the NO_2 photolysis rate), is generally shorter than its lifetime with respect to isotopic exchange (where $\tau_{\text{exchange-NO}_2} = \frac{1}{k_{\text{NO}+\text{NO}_2}[\text{NO}]}$, with $k_{\text{NO}+\text{NO}_2} = 8.4 \times 10^{-14} \text{ cm}^3 \text{ mol}^{-1} \text{ s}^{-1}$ the rate constant for the N isotopic exchange between NO and NO_2 ; Sharma et al., 1970). Therefore, ^{15}N partitioning between NO and NO_2 is limited and mainly determined by a combination of PHIFE and KIE, namely the Leighton cycle isotopic effect (LCIE). On the other hand, in polluted environments such as Fairbanks in winter, NO and NO_2 are more likely to be in isotopic equilibrium than in remote areas due to a low O_3/NO ratio (Li et al., 2020). Typically, during the daytime NO_2 collection intervals, $\tau_{\text{exchange-NO}_2}$ was much shorter than $\tau_{\text{chem-NO}_2}$ during the field campaign (Table S4 in Supporting Information S1). At night, when photolysis ceases, the EIE controls the N fractionation between NO and NO_2 , as the NO oxidation is slower. Besides, in theory, lower temperatures exacerbate the ^{15}N enrichment of NO_2 relative to NO_x emissions (Walters & Michalski, 2015). Between a LCIE- and EIE-dominated regime, all isotopic effects can be significant. In this context, and as suggested by Figure 2a, substantial N fractionation between NO and NO_2 is expected under Fairbanks winter conditions (i.e., low temperatures, weak insolation, and high- NO_x), controlled by EIE.

Under an EIE dominant regime, F_N can be expressed in a simplified form as follows (see Albertin et al., 2021 and references therein for derivation):

$$F_N \approx \frac{\alpha_{\text{EIE}(\text{NO}_2/\text{NO})} - 1}{\alpha_{\text{EIE}(\text{NO}_2/\text{NO})}} \quad (3)$$

$\alpha_{\text{EIE}(\text{NO}_2/\text{NO})}$ can be calculated using an expression derived from the Bigeleisen-Mayer equation in the harmonic oscillator approximation (Walters et al., 2016):

$$(\alpha_{\text{EIE}(\text{NO}_2/\text{NO})} - 1) \times 1000 = \frac{3.9968}{T^4} \times 10^{10} + \frac{-7.9646}{T^3} \times 10^8 + \frac{6.2144}{T^2} \times 10^6 + \frac{-0.2911}{T} \times 10^4 \quad (4)$$

with T the ambient temperature in Kelvin. We calculate theoretically predicted $\alpha_{\text{EIE}(\text{NO}_2/\text{NO})}$ values at CTC using the mean surface temperature during each NO_2 collection interval (Table S5 in Supporting Information S1). Theoretical $\alpha_{\text{EIE}(\text{NO}_2/\text{NO})}$ values range from 1.0411 to 1.0499 (Figure 2b), corresponding to the observed minimum and maximum temperatures of -32.5°C and -1.8°C , respectively, with a mean of 1.0461 ± 0.0024 . This value matches well with the value of 1.0471 ± 0.0512 derived from the observed F_N at our sampling site (45.0‰; slope of the regression line in Figure 2a and Equation 3 ($\alpha_{\text{EIE}(\text{NO}_2/\text{NO})} = \frac{1}{1 - F_N}$)). This excellent agreement between the theoretical and observation-derived $\alpha_{\text{EIE}(\text{NO}_2/\text{NO})}$, assuming an EIE-dominated regime, demonstrates that the ^{15}N partitioning between NO and NO_2 at our site is indeed mainly determined by isotopic equilibrium. Importantly, while laboratory and theoretical studies still disagree on the magnitude of $\alpha_{\text{EIE}(\text{NO}_2/\text{NO})}$ (see Li et al., 2020 for a review), our results confirm the applicability of the Walters et al. (2016) theoretical expression for $\alpha_{\text{EIE}(\text{NO}_2/\text{NO})}$ in a polar winter environment.

Since the first work of Freyer et al. (1993), a few similar investigations have been carried out at mid-latitudes. Walters et al. (2018) and Albertin et al. (2021) conducted NO_2 sampling in summer and spring, respectively, in moderately polluted atmospheres. They revealed that $\delta^{15}\text{N}(\text{NO}_2)$ was primarily driven by the variability in the $\delta^{15}\text{N}$ value of NO_x emissions. N fractionation effects were found to have little influence (below ca. 2‰) with NO_x being overwhelmingly in the form of NO_2 . In contrast, in an Alpine urban area during winter, Albertin et al. (2024) observed significant N fractionation between NO_x emissions and NO_2 , which largely explained their $\delta^{15}\text{N}(\text{NO}_2)$ record. Our results are consistent with these previous studies (see summary of $\delta^{15}\text{N}(\text{NO}_2)$ measurements in Table S6 in Supporting Information S1) and provide further observational evidence that as pollution levels rise (i.e., low f_{NO_2}), the disparity in $\delta^{15}\text{N}$ between primary NO_x and NO_2 increases due to equilibrium fractionation effects.

3.3. Identification of NO_x Emission Sources

Following the results from the previous section, the $\delta^{15}\text{N}$ value of NO_x emissions at CTC ($\delta^{15}\text{N}(\text{NO}_x)_{\text{ctc-obs_corr}}$) can be accurately derived for each of the 33 NO_2 collection intervals (14 daytime and 19 nighttime) as follows: $\delta^{15}\text{N}(\text{NO}_x)_{\text{ctc-obs_corr}} = \delta^{15}\text{N}(\text{NO}_2)_{\text{ctc-obs}} - F_N \times (1 - f_{\text{NO}_2})$ with F_N calculated from Equations 3 and 4 and using ambient temperatures at CTC (Table S3 in Supporting Information S1). $\delta^{15}\text{N}(\text{NO}_x)_{\text{ctc-obs_corr}}$ is found to vary between -16.3‰ and -7.3‰ (mean propagated error of 2.6‰ , Table S5 in Supporting Information S1), with a weighted mean (by the mean ambient NO_2 mixing ratio over the collection intervals) of $(-10.3 \pm 2.0)\text{‰}$ (Table 1). Using the relative contribution of NO_x emission sources given by the ADEC/EPA inventory over the non attainment area (Section 2.2) and $\delta^{15}\text{N}$ values reported in the literature, one can calculate the expected $\delta^{15}\text{N}$ of NO_x over this region ($\delta^{15}\text{N}(\text{NO}_x)_{\text{nonatt-calc}}$; Equation 2 with $i = \text{coal-PP, diesel-PP, wood, vehicle exhaust, gas, oil, and others}$) during each NO_2 collection interval. Power plants are large emitters of NO_x in Fairbanks (Figure S3 in Supporting Information S1). Their contribution to surface pollution is expected to vary according to atmospheric mixing conditions. According to the inventory, vehicle exhaust and oil for space heating dominated surface NO_x sources during the ALPACA-2022 winter campaign (Figure S3 in Supporting Information S1).

The literature reports a wide range of $\delta^{15}\text{N}$ values for NO_x generated by vehicle exhaust, depending on the type of fuel, the presence of an emission control system, and the engine running time (Heaton, 1990; Ammann et al., 1999; Felix & Elliott, 2014; Walters, Tharp, et al., 2015; Walters, Goodwin, et al., 2015; Miller et al., 2017; Zong et al., 2017, 2020). Reviewing $\delta^{15}\text{N}$ measurements in diverse conditions (warm-start, cold-start, running) with various vehicle types (diesel- and gasoline-powered), Song et al. (2022) reported a mean vehicle-emitted $\delta^{15}\text{N}(\text{NO}_x)$ of $(-7.1 \pm 4.2)\text{‰}$. Fossil gas combustion also emits ^{15}N -depleted NO_x , with a mean of $(-16.5 \pm 1.7)\text{‰}$ (Walters, Tharp, et al., 2015). The $\delta^{15}\text{N}$ of NO_x emitted from oil combustion (heating oil and diesel-fired boilers) is not reported in the literature. However, as for gasoline, diesel, and fossil gas, the N content of distillate oil is negligible. Therefore, NO_x emitted from oil combustion falls into the category of thermal production (i.e., NO_x produced by the breaking of N_2 at high temperature), in contrast to NO_x originating from the

Table 1

Mean $\delta^{15}\text{N}$ of NO_x at the CTC Site Fairbanks, Alaska ($\delta^{15}\text{N}(\text{NO}_x)_{\text{ctc-obs_corr}}$) and Mean $\delta^{15}\text{N}$ of NO_x Derived From the ADEC/EPA NO_x Emission Inventory ($\delta^{15}\text{N}(\text{NO}_x)_{\text{nonatt-calc}}$). $\delta^{15}\text{N}(\text{NO}_x)_{\text{ctc-obs_corr}}$ Values Were Derived From 33 Measured $\delta^{15}\text{N}$ (NO_2) Values Corrected for Equilibrium Isotopic Effects (Section 3.2). $\delta^{15}\text{N}(\text{NO}_x)_{\text{nonatt-calc}}$ Values Were Derived From Equation 2 and the ADEC/EPA NO_x Emission Inventory for Two Emission Scenarios: (a) 100% of Power Plant Emissions Mixes With Surface NO_x Emitted in the Fairbanks Non Attainment Area (All Emissions) and (b) Emissions From Coal-Fired Power Plant do Not Mix With Surface NO_x Emitted in the Fairbanks Non Attainment Area (No Coal-PP)

	(Mean $\delta^{15}\text{N}(\text{NO}_x)_{\text{ctc-obs_corr}} \pm 1\sigma$) ‰	(Mean $\delta^{15}\text{N}(\text{NO}_x)_{\text{nonatt-calc}} \pm 1\sigma$) ‰	
		All emissions	No coal-PP
Over the sampling period	-10.3 ± 2.0	3.4 ± 2.0	-12.4 ± 1.4
Daytime	-9.7 ± 1.6	3.5 ± 0.8	-11.0 ± 0.5
Nighttime	-10.71 ± 2.0	3.4 ± 2.6	-13.4 ± 0.8

Note. Emission data are reported in Table S8 and S9 in Supporting Information S1 for the “All emissions” and “No coal-PP” scenarios, respectively. The mean $\delta^{15}\text{N}(\text{NO}_x)_{\text{nonatt-calc}}$ values are weighted by the mean ambient NO_2 mixing ratio over the collection intervals. Daytime: 09:00–17:00 LT and nighttime: 17:00–09:00 LT. The mean calculation propagation error on $\delta^{15}\text{N}(\text{NO}_x)_{\text{nonatt-calc}}$ over the sampling period is 1.7 and 2.5‰ for emission scenario 1 (All emissions) and 2 (No coal-PP), respectively. Individual $\delta^{15}\text{N}(\text{NO}_x)_{\text{nonatt-calc}}$ values and propagation errors are reported in Table S11 in Supporting Information S1.

N in the fuel (Miller & Bowman, 1989). While it is difficult to estimate the $\delta^{15}\text{N}$ value of NO_x emitted by oil-fired burners (fueled with heating oil for space heating and diesel for power generation), we may expect it to lie close to diesel-powered vehicles and fossil gas burner exhausts, somewhere between ca. -20‰ and -13‰ (Walters, Tharp, et al., 2015, Walters et al., 2018). Therefore, it is reasonable to assume that the $\delta^{15}\text{N}$ value of NO_x emitted by oil combustion is approximately of $(-16.5 \pm 4.0)\text{‰}$, as for gas combustion. Coal-PP with selective catalytic reduction technology emit NO_x with the highest $\delta^{15}\text{N}$ content, averaging $(19.5 \pm 2.3)\text{‰}$ (Felix et al., 2012). We set arbitrarily $\delta^{15}\text{N}(\text{NO}_x)_{\text{others}}$ at -16.5‰ because these minor sources correspond to stationary emissions of gas and oil combustion. Based on the mean $\delta^{15}\text{N}$ of temperate forest $(-2.8 \pm 2.0)\text{‰}$; Martinelli et al., 1999) and using the empirical relationship between the $\delta^{15}\text{N}$ of burnt biomass and the $\delta^{15}\text{N}$ of NO_x determined by Chai et al. (2019), $\delta^{15}\text{N}(\text{NO}_x)_{\text{wood}}$ is estimated at $(-0.1 \pm 1.3)\text{‰}$.

In a first approach, 100% of diesel-PP and coal-PP emissions are included in the calculation of $\delta^{15}\text{N}(\text{NO}_x)_{\text{nonatt-calc}}$ for the 33 NO_2 collection intervals, resulting in a weighted mean value of $(3.4 \pm 2.0)\text{‰}$ (Table 1). It is worth pointing out that the $\delta^{15}\text{N}(\text{NO}_x)$ signature of coal combustion (ca. 20‰) is very distinct from the isotopic signatures of the other important NO_x sources (varying between ca. -7 and -17‰). As a result, the $\delta^{15}\text{N}(\text{NO}_x)$ in Fairbanks is expected to be quite sensitive to the coal-PP contribution. The Aurora and Doyon power plants are the largest emitters of NO_x from coal combustion in downtown Fairbanks (Table S7 in Supporting Information S1). With stack heights of 26 and 48 m, respectively, the top of the power plant chimneys are often above the winter surface boundary layer (ca. 25 m; Brett et al., 2024). Consequently, only a fraction of the NO_x emissions from these high stacks may be expected to reach the surface, particularly during very stable meteorological conditions with SBIs (Moon et al., 2024; Simpson et al., 2024). This is less the case for diesel-PP with lower stack heights, such as Zehnder near CTC emitting NO_x closer to the surface (18 m). Thus, when assuming 100% of coal-PP emissions mixes with surface NO_x (representing ca. 52% of the total NO_x , Table S8 in Supporting Information S1), it is not surprising that $\delta^{15}\text{N}(\text{NO}_x)_{\text{nonatt-calc}}$ values are biased high with respect to $\delta^{15}\text{N}(\text{NO}_x)_{\text{ctc-obs_corr}}$ values. This result implies that the average coal-PP contribution to surface NO_x level was likely below ca. 50% during the campaign.

In contrast, if the fraction of coal-PP emissions reaching the Fairbanks surface is assumed to be negligible (i.e., no mixing down of coal-PP plumes, Table S9 in Supporting Information S1), the weighted mean $\delta^{15}\text{N}(\text{NO}_x)_{\text{nonatt-calc}}$ over the NO_2 sampling periods is $(-12.4 \pm 1.4)\text{‰}$, matching well with the mean $\delta^{15}\text{N}(\text{NO}_x)_{\text{ctc-obs_corr}}$ (Table 1). Note that over the entire ALPACA-2022 campaign, the mean $\delta^{15}\text{N}(\text{NO}_x)_{\text{nonatt-calc}}$ is similar (-12.1‰). These results suggest that the inventory of NO_x emissions for the Fairbanks nonattainment area is reasonably representative of emissions at CTC, including emissions from diesel-PP, and that NO_x emissions from coal-PP may only be contributing marginally to breathing NO_x levels in downtown Fairbanks. Note that the sample of $\delta^{15}\text{N}(\text{NO}_x)_{\text{nonatt-calc}}$ values is not significantly different from that of $\delta^{15}\text{N}(\text{NO}_x)_{\text{ctc-obs_corr}}$ values (p value > 0.05), until more than 5% of coal-PP are included. In other words, if, on average, during the NO_2 collection intervals, up to 5%

of coal-PP emissions had reached the surface at CTC, the impact on the ambient NO_x isotopic signature is too small to be detected robustly because of the dispersion in the comparison between observed and calculated values. In the scenario where 5% of coal-PP emissions reach the surface layer, coal-PP emissions account for $(5.0 \pm 1.3)\%$ of total NO_x emissions, while vehicle exhaust and heating oil combustion contribute $(34.0 \pm 15.1)\%$ and $(29.0 \pm 7.5)\%$, respectively (Table S10 in Supporting Information S1). It is interesting to note that, without coal-PP contribution to surface NO_x , the weighted mean daytime and nighttime $\delta^{15}\text{N}(\text{NO}_x)_{\text{nonatt-calc}}$ is slightly different $((-11.0 \pm 0.5)\text{‰}$ and $(-13.4 \pm 0.8)\text{‰}$, respectively), as for $\delta^{15}\text{N}(\text{NO}_x)_{\text{ctc-obs_corr}}$ $((-9.7 \pm 1.6)\text{‰}$ and $(-10.7 \pm 2.0)\text{‰}$, respectively). This diurnal sensitivity of $\delta^{15}\text{N}(\text{NO}_x)$ values likely reflects the increase in the oil-combustion contribution (mainly from space heating) to total NO_x emissions at night, while the vehicle exhaust contribution decreases (Figure S3 in Supporting Information S1). These results support our hypothesis that the $\delta^{15}\text{N}(\text{NO}_x)_{\text{oil}}$ is rather low compared to the $\delta^{15}\text{N}(\text{NO}_x)_{\text{vehicle}}$.

Quantifying the amount of power plant emissions reaching the surface in downtown Fairbanks is relevant to the design of pollution control strategies. The fraction of coal-PP emissions ($x_{\text{coal-PP_ctc}}$) that reached the CTC surface site during the NO_2 sampling periods can be derived from Equation 2 (see Text S1 in Supporting Information S1) following

$$x_{\text{coal-PP_ctc}} = \frac{\sum_{j \neq \text{coal-PP}} (E_j \times \delta^{15}\text{N}(\text{NO}_x)_j) - \sum_{j \neq \text{coal-PP}} E_j \times \delta^{15}\text{N}(\text{NO}_x)_{\text{ctc-obs_corr}}}{E_{\text{coal-PP}} \times (\delta^{15}\text{N}(\text{NO}_x)_{\text{ctc-obs_corr}} - \delta^{15}\text{N}(\text{NO}_x)_{\text{coal-PP}})} \quad (5)$$

with $E_{\text{coal-PP}}$ the total amount of NO_x emitted by coal-fired power plants in the vicinity of CTC. However, it is not possible to precisely estimate $x_{\text{coal-PP_ctc}}$ at the CTC site from our analysis, as the error propagation in Equation 5 of isotopic fractionation and $\delta^{15}\text{N}$ values of individual emission sources generates a large uncertainty. For example, $\delta^{15}\text{N}(\text{NO}_x)$ of vehicle exhaust, the reported dominant source, could be overestimated in our analysis due to the unusual winter environmental conditions prevailing in Fairbanks. Cold engines emit ^{15}N -depleted NO_x , generally below ca. -9‰ , compared to running vehicles (Walters, Goodwin, et al., 2015; Zong et al., 2020). During winter in Fairbanks, low ambient temperatures, typically below -15°C (Figure S2 in Supporting Information S1), engender short vehicle trips with frequent cold starts. Given that 60%–80% of NO_x from a typical vehicle is emitted during the first 200 s of cold start operation (Walters, Goodwin, et al., 2015), $\delta^{15}\text{N}(\text{NO}_x)_{\text{vehicle}}$ in Fairbanks could lie in the lower range of isotopic signatures reported for motor engines. The proportion of diesel and gasoline vehicle is also a source of uncertainty for $\delta^{15}\text{N}(\text{NO}_x)_{\text{vehicle}}$. Indeed, more negative $\delta^{15}\text{N}(\text{NO}_x)_{\text{vehicle}}$ have been reported for diesel (from -23.3 to -15.9‰) compared to gasoline vehicle emissions (from -15.1 to 10.5‰) (Walters, Goodwin, et al., 2015; Walters, Tharp, et al., 2015; Zong et al., 2020). Diesel vehicles accounted for an estimated 10% of the total fleet in the Fairbanks nonattainment area in winter 2022 but contributed 59% of on-road emissions (Table S12 in Supporting Information S1). In addition, according to Brett et al. (2024), diesel vehicle NO_x emissions may be underestimated in very cold conditions during the winter in Fairbanks. Although observed $\delta^{15}\text{N}(\text{NO}_x)$ at CTC is quite well reproduced using a mean $\delta^{15}\text{N}(\text{NO}_x)_{\text{vehicle}}$ of -7.1‰ , specific conditions in Fairbanks could punctually lower this value during rush hours and in cold conditions.

Despite these uncertainties, we attempt to estimate an upper limit of $x_{\text{coal-PP_ctc}}$ using the lower limits in the uncertainty ranges of NO_x emission source $\delta^{15}\text{N}$ -signature (i.e., $\delta^{15}\text{N}(\text{NO}_x)_i = \text{mean value} - 1\sigma$) in order to maximize the coal-PP contribution to CTC. Using $\delta^{15}\text{N}(\text{NO}_x)_{\text{ctc-obs_corr}}$ values and average emission rates over corresponding NO_2 collection intervals, the mean maximum $x_{\text{coal-PP_ctc}}$ over the sampling campaign is of ca. 22%. Mixed with surface emissions, it represents an average maximum contribution of coal-PP to the surface NO_x at CTC of ca. 18%. Note that a higher contribution of vehicle exhaust emissions to CTC would give a lower contribution of coal-PP. This maximum coal-PP contribution is derived with emissions averaged over the NO_2 collection intervals. It is therefore likely that, during shorter periods of time, and depending on the meteorological conditions, coal combustion emissions from elevated power plants could have mixed more with ambient NO_x at the surface, as suggested by Brett et al. (2024). Complementary investigations are required to quantify the high-time resolved contribution of power plant emissions on the surface NO_x budget in downtown Fairbanks in winter.

4. Conclusions

Consistent with prior studies in mid-latitude urban areas, the N isotopic composition of atmospheric NO_2 in polluted wintertime Fairbanks exhibited large temporal variations driven by N fractionation between NO and

NO₂. The N isotopic fractionation is found to be driven by the equilibrium effect between NO and NO₂, at rates in excellent agreement with the theoretical predictions. This result confirms that N partitioning between NO and NO₂ is well-constrained across diverse polluted environments and that the resulting N fractionation can be accurately predicted. This holds significant implications for understanding $\delta^{15}\text{N}$ dynamics in the atmospheric N_r cycle, in particular for the accuracy of $\delta^{15}\text{N}$ -based identification and apportionment of NO_x emission sources. Nonetheless, uncertainties pertain to the $\delta^{15}\text{N}$ of individual emission sources, representing a primary limitation in $\delta^{15}\text{N}$ -based source apportionment. Efforts should focus on measuring accurately these $\delta^{15}\text{N}$ -signatures, notably for vehicle exhaust and heating oil combustion, while accounting for environmental conditions and emission control technologies.

Our isotopic analysis indicates that the very large emissions from coal-fired power plants with elevated stacks do not appear to contribute substantially to NO_x levels in the Fairbanks urban center, likely well below 18% on average. To our knowledge, this is the first quantitative estimate of the coal-power plants contribution to NO_x surface levels in this area. This result suggests that, on average, there is relatively little mixing between the surface boundary layer and above in winter Fairbanks. In addition, this study shows that vehicle exhaust and oil combustion from space heating were the dominant NO_x sources at our sampling site. Our results align well with previous findings indicating that Fairbanks downtown pollution is largely influenced by surface emissions (Moon et al., 2024; Simpson et al., 2024).

We wish to emphasize that such an analysis of the NO₂ isotopic composition is very valuable and even necessary for the interpretation of $\delta^{15}\text{N}$ records of NO₃[−] in urban atmospheres. Given its critical contribution to air quality, atmospheric samples of NO₃[−] are widely used in the literature to trace NO_x emission sources using $\delta^{15}\text{N}$ measurements. However, to date, there is a limited understanding of possible N isotopic effects between NO₂ and NO₃[−]. Chang et al. (2018) estimated that NO₃[−] isotope-based source apportionment studies conducted in China overestimated the contribution of coal combustion by ca. 30% on average when N isotopic fractionation effects were not accounted for. Although most recent studies do apply some isotopic fractionation correction to $\delta^{15}\text{N}$ (NO₃[−]) records (e.g., Bekker et al., 2023; Fan et al., 2023; Li et al., 2022; Lim et al., 2022; Zhang et al., 2022), we currently suffer from a too limited number of simultaneous $\delta^{15}\text{N}$ measurements in atmospheric NO₂ and NO₃[−] to assess the applicability of these theoretical corrections to various ambient conditions (see Albertin et al., 2024). Therefore, relying only on $\delta^{15}\text{N}$ measurements of NO₃[−] to trace NO_x emission sources in urban settings remains uncertain. In parallel with NO₂ sampling, we collected atmospheric NO₃[−] in and outside Fairbanks throughout the ALPACA-2022 campaign ($n = 95$ at sampling time resolution ranging from half a day to a few hours). An in-depth analysis of the factors influencing the NO₃[−] isotopic composition, notably the NO₂ isotopic composition, f_{NO_2} , and temperature, will be conducted in a forthcoming study. Implications for the traceability of NO₃[−] chemistry processes and sources from isotopic records will also be assessed. At the same time, we encourage other groups to carry out more simultaneous $\delta^{15}\text{N}$ measurements of NO₂ and NO₃[−] under other atmospheric conditions to improve further our understanding of N isotopic fractionation effects and be more confident in accounting for them in quantitative apportionment of N_r emission sources and processes from NO₃[−] records.

Data Availability Statement

Hourly meteorological and trace gas data from the ALPACA-2022 study are available to the scientific community through the ALPACA data portal hosted by Arcticdata.io (<https://arcticdata.io/catalog/portals/ALPACA/Data>). Data from this study (i.e., hourly NO_x emission rates from the updated ADEC/EPA inventory and isotopic measurements) are available at <https://doi.org/10.18739/A2XG9FC9F> (Albertin et al., 2024). A copy of isotopic measurements as well as meteorological and trace gas measurements, and ADEC/EPA emission data averaged over each denuder collection interval is available in Supporting Information S1.

References

- ADEC. (2019a). In *Alaska department of environmental conservation (ADEC) - amendments to: State air quality control plan* (Vol. III). Retrieved from <https://dec.alaska.gov/air/anpms/communities/fbks-pm2-5-serious-sip/>
- ADEC. (2019b). *Alaska department of environmental conservation - state air quality control plan. Executive summary*. Retrieved from <https://dec.alaska.gov/air/anpms/communities/fbks-pm2-5-serious-sip/>
- Albertin, S., Bekki, S., Savarino, J., Brett, N., Law, K. S., Cesler-Maloney, M., et al. (2024). *Nitrogen isotope measurements of nitrogen dioxide in Fairbanks, Alaska, during the Alaskan Layered Pollution And Chemical Analysis (ALPACA) 2022 field study*. Arctic Data Center. <https://doi.org/10.18739/A2XG9FC9F>

Acknowledgments

This research benefited from national and IGE infrastructures and laboratory platforms, RéGEF and PANDA respectively and has received funding from: The Agence Nationale de la Recherche (ANR) via contract ANR-21-CE01-0017 CASPA (coordinated by Kathy Law), the Institut polaire français Paul-Emile Victor (IPEV) (Grant 1215), INSU-CNRS (National Institute of Sciences of the Universe) via its national LEFE program (Les Enveloppes Fluides et l'Environnement), the Labex OSUG@2020 (Investissements d'avenir – ANR10 LABX56), and IDEX-UGA ANR project ANR-15-IDEX-02 (coordinated by Joël Savarino). BA acknowledges NOAA Grant NA20OAR4310295. The authors thank the power plant facilities for providing their emission data. The authors particularly acknowledge Deanna Huff (ADEC) and Kathleen Fahey (EPA) for providing the updated ALPACA-2022 emission inventory. The authors are very grateful to the University of Alaska Fairbanks and the Geophysical Institute, the ALPACA participants, and the technical and administrative staff of IGE and LATMOS for assistance.

- Albertin, S., Savarino, J., Bekki, S., Barbero, A., & Caillon, N. (2021). Measurement report: Nitrogen isotopes ($\delta^{15}\text{N}$) and first quantification of oxygen isotope anomalies ($\Delta^{17}\text{O}$, $\delta^{18}\text{O}$) in atmospheric nitrogen dioxide. *Atmospheric Chemistry and Physics*, 21(13), 10477–10497. <https://doi.org/10.5194/acp-21-10477-2021>
- Albertin, S., Savarino, J., Bekki, S., Barbero, A., Grilli, R., Fournier, Q., et al. (2024). Diurnal variations in oxygen and nitrogen isotopes of atmospheric nitrogen dioxide and nitrate: Implications for tracing NO_x oxidation pathways and emission sources. *Atmospheric Chemistry and Physics*, 24(2), 1361–1388. <https://doi.org/10.5194/acp-24-1361-2024>
- Altieri, K. E., Burger, J., Language, B., & Piketh, S. J. (2022). A case study in the wintertime Vaal Triangle Air-Shed Priority Area on the utility of the nitrogen stable isotopic composition of aerosol nitrate to identify NO_x sources. *Clean Air Journal*, 32(1). <https://doi.org/10.17159/caj/2022/32/1.12505>
- Ammann, M., Siegwolf, R., Pichlmayer, F., Suter, M., Saurer, M., & Brunold, C. (1999). Estimating the uptake of traffic-derived NO_2 from ^{15}N abundance in Norway spruce needles. *Oecologia*, 118(2), 124–131. <https://doi.org/10.1007/s004420050710>
- Begun, G. M., & Fletcher, W. H. (1960). Partition function ratios for molecules containing nitrogen isotopes. *The Journal of Chemical Physics*, 33(4), 1083–1085. <https://doi.org/10.1063/1.1731338>
- Begun, G. M., & Melton, C. E. (1956). Nitrogen isotopic fractionation between NO and NO_2 and mass discrimination in mass analysis of NO_2 . *The Journal of Chemical Physics*, 25(6), 1292–1293. <https://doi.org/10.1063/1.1743215>
- Bekker, C., Walters, W. W., Murray, L. T., & Hastings, M. G. (2023). Nitrate chemistry in the northeast US – Part 1 Nitrogen isotope seasonality tracks nitrate formation chemistry. *Atmospheric Chemistry and Physics*, 23(7), 4185–4201. <https://doi.org/10.5194/acp-23-4185-2023>
- Blum, D. E., Walters, W. W., Eris, G., Takeuchi, M., Huey, L. G., Tanner, D., et al. (2023). Collection of nitrogen dioxide for nitrogen and oxygen isotope determination—laboratory and environmental chamber evaluation. *Analytical Chemistry*, 95(6), 3371–3378. <https://doi.org/10.1021/acs.analchem.2c04672>
- Brett, N., Law, K. S., Arnold, S. R., Fochesatto, J. G., Raut, J.-C., Onishi, T., et al. (2024). Investigating processes influencing simulation of local Arctic wintertime anthropogenic pollution in Fairbanks, Alaska during ALPACA-2022 (pp. 1–55). EGU sphere. <https://doi.org/10.5194/egusphere-2024-1450>
- Cesler-Maloney, M., Simpson, W. R., Miles, T., Mao, J., Law, K. S., & Roberts, T. J. (2022). Differences in ozone and particulate matter between ground level and 20 m aloft are frequent during wintertime surface-based temperature inversions in Fairbanks, Alaska. *Journal of Geophysical Research: Atmospheres*, 127(10), e2021JD036215. <https://doi.org/10.1029/2021JD036215>
- Chai, J., Miller, D. J., Scheuer, E., Dibb, J., Selimovic, V., Yokelson, R., et al. (2019). Isotopic characterization of nitrogen oxides (NO_x), nitrous acid (HONO), and nitrate (pNO_3^-) from laboratory biomass burning during FIREX. *Atmospheric Measurement Techniques*, 12(12), 6303–6317. <https://doi.org/10.5194/amt-12-6303-2019>
- Chang, Y., Zhang, Y., Tian, C., Zhang, S., Ma, X., Cao, F., et al. (2018). Nitrogen isotope fractionation during gas-to-particle conversion of NO_x to NO_3^- in the atmosphere – Implications for isotope-based NO_x source apportionment. *Atmospheric Chemistry and Physics*, 18(16), 11647–11661. <https://doi.org/10.5194/acp-18-11647-2018>
- Crutzen, P. J. (1970). The influence of nitrogen oxides on the atmospheric ozone content. *Quarterly Journal of the Royal Meteorological Society*, 96(408), 320–325. <https://doi.org/10.1002/qj.49709640815>
- Fan, M.-Y., Zhang, W., Zhang, Y.-L., Li, J., Fang, H., Cao, F., et al. (2023). Formation mechanisms and source apportionments of nitrate aerosols in a megacity of eastern China based on multiple isotope observations. *Journal of Geophysical Research Atmospheres*, 128(6), e2022JD038129. <https://doi.org/10.1029/2022JD038129>
- Felix, J. D., & Elliott, E. M. (2014). Isotopic composition of passively collected nitrogen dioxide emissions: Vehicle, soil and livestock source signatures. *Atmospheric Environment*, 92, 359–366. <https://doi.org/10.1016/j.atmosenv.2014.04.005>
- Felix, J. D., Elliott, E. M., & Shaw, S. L. (2012). Nitrogen isotopic composition of coal-fired power plant NO_x : Influence of emission controls and implications for global emission inventories. *Environmental Science & Technology*, 46(6), 3528–3535. <https://doi.org/10.1021/es203355v>
- Fochesatto, G. J., Mayfield, J. A., Starkenburg, D. P., Gruber, M. A., & Conner, J. (2015). Occurrence of shallow cold flows in the winter atmospheric boundary layer of interior of Alaska. *Meteorology and Atmospheric Physics*, 127(4), 369–382. <https://doi.org/10.1007/s00703-013-0274-4>
- Freyer, H. D., Kley, D., Volz-Thomas, A., & Kobel, K. (1993). On the interaction of isotopic exchange processes with photochemical reactions in atmospheric oxides of nitrogen. *Journal of Geophysical Research*, 98(D8), 14791–14796. <https://doi.org/10.1029/93JD00874>
- Galloway, J. N., Townsend, A. R., Erisman, J. W., Bekunda, M., Cai, Z., Freney, J. R., et al. (2008). Transformation of the nitrogen cycle: Recent trends, questions, and potential solutions. *Science*, 320(5878), 889–892. <https://doi.org/10.1126/science.1136674>
- Heaton, T. H. E. (1990). $^{15}\text{N}/^{14}\text{N}$ ratios of NO_x from vehicle engines and coal-fired power stations. *Tellus B: Chemical and Physical Meteorology*, 42(3), 304–307. <https://doi.org/10.1034/j.1600-0889.1990.00007.x-1>
- Kaiser, J., Hastings, M. G., Houlton, B. Z., Röckmann, T., & Sigman, D. M. (2007). Triple oxygen isotope analysis of nitrate using the denitrifier method and thermal decomposition of N_2O . *Analytical Chemistry*, 79(2), 599–607. <https://doi.org/10.1021/ac061022s>
- Leighton, P. A. (1961). *Photochemistry of air pollution* (Vol. 66). Academic Press.
- Li, J., Zhang, X., Orlando, J., Tyndall, G., & Michalski, G. (2020). Quantifying the nitrogen isotope effects during photochemical equilibrium between NO and NO_2 : Implications for $\delta^{15}\text{N}$ in tropospheric reactive nitrogen. *Atmospheric Chemistry and Physics*, 20(16), 9805–9819. <https://doi.org/10.5194/acp-20-9805-2020>
- Li, Y., Shi, G., Chen, Z., Lan, M., Ding, M., Li, Z., & Hastings, M. G. (2022). Significant latitudinal gradient of nitrate production in the marine atmospheric boundary layer of the northern hemisphere. *Geophysical Research Letters*, 49(23), e2022GL100503. <https://doi.org/10.1029/2022GL100503>
- Lim, S., Lee, M., Savarino, J., & Laj, P. (2022). Oxidation pathways and emission sources of atmospheric particulate nitrate in Seoul: Based on $\delta^{15}\text{N}$ and $\Delta^{17}\text{O}$ measurements. *Atmospheric Chemistry and Physics*, 22(8), 5099–5115. <https://doi.org/10.5194/acp-22-5099-2022>
- Martinelli, L. A., Piccolo, M. C., Townsend, A. R., Vitousek, P. M., Cuevas, E., McDowell, W., et al. (1999). Nitrogen stable isotopic composition of leaves and soil: Tropical versus temperate forests. *Biogeochemistry*, 46(1/3), 45–65. <https://doi.org/10.1023/A:1006100128782>
- Mayfield, J. A., & Fochesatto, G. J. (2013). The layered structure of the winter atmospheric boundary layer in the interior of Alaska. *Journal of Applied Meteorology and Climatology*, 52(4), 953–973. <https://doi.org/10.1175/JAMC-D-12-01.1>
- McIlvin, M. R., & Altabet, M. A. (2005). Chemical conversion of nitrate and nitrite to nitrous oxide for nitrogen and oxygen isotopic analysis in freshwater and seawater. *Analytical Chemistry*, 77(17), 5589–5595. <https://doi.org/10.1021/ac050528s>
- Miller, C. E., & Yung, Y. L. (2000). Photo-induced isotopic fractionation. *Journal of Geophysical Research*, 105(D23), 29039–29051. <https://doi.org/10.1029/2000JD900388>
- Miller, D. J., Chai, J., Guo, F., Dell, C. J., Karsten, H., & Hastings, M. G. (2018). Isotopic composition of in situ soil NO_x emissions in manure-fertilized cropland. *Geophysical Research Letters*, 45(21), 12058–12066. <https://doi.org/10.1029/2018GL079619>

- Miller, D. J., Wojtal, P. K., Clark, S. C., & Hastings, M. G. (2017). Vehicle NO_x emission plume isotopic signatures: Spatial variability across the eastern United States. *Journal of Geophysical Research: Atmospheres*, 122(8), 4698–4717. <https://doi.org/10.1002/2016JD025877>
- Miller, J. A., & Bowman, C. T. (1989). Mechanism and modeling of nitrogen chemistry in combustion. *Progress in Energy and Combustion Science*, 15(4), 287–338. [https://doi.org/10.1016/0360-1285\(89\)90017-8](https://doi.org/10.1016/0360-1285(89)90017-8)
- Monse, E. U., Spindel, W., & Stern, M. J. (1969). Analysis of isotope-effect calculations illustrated with exchange equilibria among oxynitrogen compounds. In *Isotope effects in chemical processes* (Vol. 89, pp. 148–184). <https://doi.org/10.1021/ba-1969-0089.ch009>
- Moon, A., Jongebloed, U., Dingilian, K. K., Schauer, A. J., Chan, Y.-C., Cesler-Maloney, M., et al. (2024). Primary sulfate is the dominant source of particulate sulfate during winter in Fairbanks, Alaska. *ACS ES&T Air*, 1(3), 139–149. <https://doi.org/10.1021/acsestair.3c00023>
- Morin, S., Savarino, J., Frey, M. M., Domine, F., Jacobi, H.-W., Kaleschke, L., & Martins, J. M. F. (2009). Comprehensive isotopic composition of atmospheric nitrate in the Atlantic Ocean boundary layer from 65°S to 79°N. *Journal of Geophysical Research*, 114(D5). <https://doi.org/10.1029/2008JD010696>
- Nash, T. (1970). An efficient absorbing reagent for nitrogen dioxide. *Atmospheric Environment*, 4(6), 661–665. [https://doi.org/10.1016/0004-6981\(70\)90039-9](https://doi.org/10.1016/0004-6981(70)90039-9)
- Robinson, E. S., Cesler-Maloney, M., Tan, X., Mao, J., Simpson, W., & DeCarlo, P. F. (2023). Wintertime spatial patterns of particulate matter in Fairbanks, AK during ALPACA 2022. *Environmental Sciences: Atmosphere*, 3(3), 568–580. <https://doi.org/10.1039/D2EA00140C>
- Sharma, H. D., Jervis, R. E., & Wong, K. Y. (1970). Isotopic exchange reactions in nitrogen oxides. *The Journal of Physical Chemistry A*, 74(4), 923–933. <https://doi.org/10.1021/j100699a044>
- Simpson, W. R., Mao, J., Fochesatto, G. J., Law, K. S., DeCarlo, P. F., Schmale, J., et al. (2024). Overview of the alaskan layered pollution and chemical analysis (ALPACA) field experiment. *ACS ES&T Air*, 1(3), 200–222. <https://doi.org/10.1021/acsestair.3c00076>
- Song, W., Liu, X., & Liu, C. (2021). New constraints on isotopic effects and major sources of nitrate in atmospheric particulates by combining $\delta^{15}\text{N}$ and $\Delta^{17}\text{O}$ signatures. *Journal of Geophysical Research: Atmospheres*, 126(16). <https://doi.org/10.1029/2020JD034168>
- Song, W., Liu, X.-Y., Houlton, B. Z., & Liu, C.-Q. (2022). Isotopic constraints confirm the significant role of microbial nitrogen oxides emissions from the land and ocean environment. *National Science Review*, 9(9), nwac106. <https://doi.org/10.1093/nsr/nwac106>
- Song, W., Liu, X.-Y., Hu, C.-C., Chen, G.-Y., Liu, X.-J., Walters, W. W., et al. (2021). Important contributions of non-fossil fuel nitrogen oxides emissions. *Nature Communications*, 12(1), 243. <https://doi.org/10.1038/s41467-020-20356-0>
- Sutton, E. M. A., Howard, C. M., Erisman, J. W., Billen, G., & Bleeker, A. (2011). *The European nitrogen assessment, sources, effects and policy perspectives* (Vol. 30). Cambridge University Press.
- Szopa, S., Naik, V., Adhikary, B., Artaxo, P., Bernsten, T., Collins, W. D., et al. (2021). Short-lived climate forcers. In V. Masson-Delmotte, P. Zhai, A. Pirani, S. L. Connors, C. Péan, S. Berger, et al. (Eds.), *Climate change 2021: The physical science basis. Contribution of working group I to the sixth assessment report of the intergovernmental panel on climate change* (pp. 817–922). Cambridge University Press. <https://doi.org/10.1017/9781009157896.008>
- Tran, H. N. Q., & Mölders, N. (2011). Investigations on meteorological conditions for elevated $\text{PM}_{2.5}$ in Fairbanks, Alaska. *Atmospheric Research*, 99(1), 39–49. <https://doi.org/10.1016/j.atmosres.2010.08.028>
- Vitousek, P. M., Aber, J. D., Howarth, R. W., Likens, G. E., Matson, P. A., Schindler, D. W., et al. (1997). Human alteration of the global nitrogen cycle: Sources and consequences. *Ecological Applications*, 7(3), 737–750. [https://doi.org/10.1890/1051-0761\(1997\)007\[0737:HAOTGN\]2.0.CO;2](https://doi.org/10.1890/1051-0761(1997)007[0737:HAOTGN]2.0.CO;2)
- Walters, W. W., Fang, H., & Michalski, G. (2018). Summertime diurnal variations in the isotopic composition of atmospheric nitrogen dioxide at a small midwestern United States city. *Atmospheric Environment*, 179, 1–11. <https://doi.org/10.1016/j.atmosenv.2018.01.047>
- Walters, W. W., Goodwin, S. R., & Michalski, G. (2015). Nitrogen stable isotope composition ($\delta^{15}\text{N}$) of vehicle-emitted NO_x . *Environmental Science & Technology*, 49(4), 2278–2285. <https://doi.org/10.1021/es505580v>
- Walters, W. W., & Michalski, G. (2015). Theoretical calculation of nitrogen isotope equilibrium exchange fractionation factors for various NO_y molecules. *Geochimica et Cosmochimica Acta*, 164, 284–297. <https://doi.org/10.1016/j.gca.2015.05.029>
- Walters, W. W., Simonini, D. S., & Michalski, G. (2016). Nitrogen isotope exchange between NO and NO_2 and its implications for $\delta^{15}\text{N}$ variations in tropospheric NO_x and atmospheric nitrate. *Geophysical Research Letters*, 43(1), 440–448. <https://doi.org/10.1002/2015GL066438>
- Walters, W. W., Sharp, B. D., Fang, H., Kozak, B. J., & Michalski, G. (2015). Nitrogen isotope composition of thermally produced NO_x from various fossil-fuel combustion sources. *Environmental Science & Technology*, 49(19), 11363–11371. <https://doi.org/10.1021/acs.est.5b02769>
- Whaley, C. H., Law, K. S., Hjorth, J. L., Skov, H., Arnold, S. R., Langner, J., et al. (2023). Arctic tropospheric ozone: Assessment of current knowledge and model performance. *Atmospheric Chemistry and Physics*, 23(1), 637–661. <https://doi.org/10.5194/acp-23-637-2023>
- WHO. (2021). *World health organization global air quality guidelines: Particulate matter ($\text{PM}_{2.5}$ and PM_{10}), ozone, nitrogen dioxide, sulfur dioxide and carbon monoxide*. World Health Organization.
- Xiao, H., Ding, S.-Y., Ji, C.-W., Li, Q.-K., & Li, X.-D. (2023). Strict control of biomass burning inhibited particulate matter nitrate pollution over Tianjin: Perspective from dual isotopes of nitrate. *Atmospheric Environment*, 293, 119460. <https://doi.org/10.1016/j.atmosenv.2022.119460>
- Young, E. D., Galy, A., & Nagahara, H. (2002). Kinetic and equilibrium mass-dependent isotope fractionation laws in nature and their geochemical and cosmochemical significance. *Geochimica et Cosmochimica Acta*, 66(6), 1095–1104. [https://doi.org/10.1016/S0016-7037\(01\)00832-8](https://doi.org/10.1016/S0016-7037(01)00832-8)
- Zhang, R., Wang, G., Guo, S., Zamora, M. L., Ying, Q., Lin, Y., et al. (2015). Formation of urban fine particulate matter. *Chemical Reviews*, 115(10), 3803–3855. <https://doi.org/10.1021/acs.chemrev.5b00067>
- Zhang, W., Bi, X., Zhang, Y., Wu, J., & Feng, Y. (2022). Diesel vehicle emission accounts for the dominate NO_x source to atmospheric particulate nitrate in a coastal city: Insights from nitrate dual isotopes of $\text{PM}_{2.5}$. *Atmospheric Research*, 278, 106328. <https://doi.org/10.1016/j.atmosres.2022.106328>
- Zhou, T., Jiang, Z., Zhou, J., Zhao, W., Wu, Y., Yu, H., et al. (2022). Fast and efficient atmospheric NO_2 collection for isotopic analysis by a 3D-printed denuder system. *Analytical Chemistry*, 94(38), 13215–13222. <https://doi.org/10.1021/acs.analchem.2c02839>
- Zong, Z., Sun, Z., Xiao, L., Tian, C., Liu, J., Sha, Q., et al. (2020). Insight into the variability of the nitrogen isotope composition of vehicular NO_x in China. *Environmental Science & Technology*, 54(22), 14246–14253. <https://doi.org/10.1021/acs.est.0c04749>
- Zong, Z., Wang, X., Tian, C., Chen, Y., Fang, Y., Zhang, F., et al. (2017). First assessment of NO_x sources at a regional background site in north China using isotopic analysis linked with modeling. *Environmental Science and Technology*, 51(11), 5923–5931. <https://doi.org/10.1021/acs.est.6b06316>

Erratum

The originally published version of this article contained typographical errors. In the second sentence of the second paragraph of the Introduction, the equation “ $(\delta^{15}\text{N} = (15/^{14}\text{N})_{\text{sample}} / (15/^{14}\text{N})_{\text{N}_2\text{-air}} - 1)$ ” should be changed to $(\delta^{15}\text{N} = (15\text{N}/^{14}\text{N})_{\text{sample}} / (15\text{N}/^{14}\text{N})_{\text{N}_2\text{-air}} - 1)$. In the fourth sentence of the fourth paragraph of Section 3.2, the equation $(\alpha_{\text{EIE}(\text{NO}_2/\text{NO})} = \frac{1}{1 - F_{\text{N}}})$ should be changed to $(\alpha_{\text{EIE}(\text{NO}_2/\text{NO})} = \frac{1}{1 - F_{\text{N}}})$. In the first sentence of the first paragraph of Section 3.3, the equation $\delta^{15}\text{N}(\text{NO}_x)_{\text{ctc-obs_corr}} = \delta^{15}\text{N}(\text{NO}_2)_{\text{ctc-obs}} - F_{\text{N}} \times (1 - 2021f_{\text{NO}_2})$ should be changed to “ $\delta^{15}\text{N}(\text{NO}_x)_{\text{ctc-obs_corr}} = \delta^{15}\text{N}(\text{NO}_2)_{\text{ctc-obs}} - F_{\text{N}} \times (1 - f_{\text{NO}_2})$ ”. The errors have been corrected, and this may be considered the authoritative version of record.